SCIENTIFIC REPORTS

OPEN

SUBJECT AREAS:
NANOPARTICLES
MECHANISM OF ACTION

Received
18 March 2014

Accepted
14 May 2014

Published
14 July 2014

Correspondence and requests for materials should be addressed to Q.S.W. (qswu@tongji.edu.cn)

A residue-free green synergistic antifungal nanotechnology for pesticide *thiram* by ZnO nanoparticles

Jingzhe Xue[1], Zhihui Luo[1], Ping Li[1], Yaping Ding[2], Yi Cui[3] & Qingsheng Wu[1]

[1]Department of Chemistry, Key Laboratory of Yangtze River Water Environment, Ministry of Education, Tongji University, Shanghai 200092, P. R. China, [2]Department of Chemistry, Shanghai University, Shanghai 200444, P. R. China, [3]Department of Materials Science and Engineering, Stanford University, Stanford, California 94305, USA.

Here we reported a residue-free green nanotechnology which synergistically enhance the pesticides efficiency and successively eliminate its residue. We built up a composite antifungal system by a simple pre-treating and assembling procedure for investigating synergy. Investigations showed 0.25 g/L ZnO nanoparticles (NPs) with 0.01 g/L *thiram* could inhibit the fungal growth in a synergistic mode. More importantly, the 0.25 g/L ZnO NPs completely degraded 0.01 g/L *thiram* under simulated sunlight irradiation within 6 hours. It was demonstrated that the formation of ZnO-*thiram* antifungal system, electrostatic adsorption of ZnO NPs to fungi cells and the cellular internalization of ZnO-*thiram* composites played important roles in synergy. Oxidative stress test indicated ZnO-induced oxidative damage was enhanced by *thiram* that finally result in synergistic antifungal effect. By reducing the pesticides usage, this nanotechnology could control the plant disease economically, more significantly, the following photocatalytic degradation of pesticide greatly benefit the human social by avoiding negative influence of pesticide residue on public health and environment.

In order to feed the expanding global population, the traditional organic pesticides were intensively used in modern agricultural production to maintain high crop yields[1]. However, doing that without negative influence on environment[2,3] and public health[4–6] is still a great challenge[7]. Luckily, the rapid development of nanotechnology provides the alternative strategies to achieve such goals. The inorganic NPs such as Ag, CuO, MgO and ZnO have been demonstrated effective antimicrobial activities singly[8–13] or combined with organic drugs[14,15] in previous studies. However, to the best of our knowledge, few papers have studied the combined antimicrobial effect of inorganic NPs with organic pesticides for plant protection, let alone demonstrated synergistic effect. It is meaningful to investigate the joint effect of such combination for increasing antimicrobial activity, reducing pesticide usage and delaying the development of resistance[16]. More importantly, for semiconductor NPs, the combination also provides the feasibility to eliminate the pesticide residue due to the photocatalytic activity. Therefore, it prompted us to set up a novel green nanotechnology which control pathogen microorganism with a synergistic antimicrobial activity and successive photocatalytic degrade pesticide residue to protect plant efficiently and environmental friendly. Such goals led us to focus on ZnO NPs which are cheap, stable[17], sensitive to pathogen fungi[18,19], biocompatibility to human cells[18,20,21] and have the essential excellent photocatalytic activity[22].

Some reports indicated the bonding between antibiotics and NPs could result in synergistic effect[14,23]. From this point of view, we envisaged *thiram*, a widely used dithiocarbamate pesticide, could bind with Zn atoms at ZnO crystal surface to form composite antifungal system for the sulfur atoms in its structure and therefore cause more destruction effect by increasing local concentration of the antimicrobial agents[14]. Thus, *thiram* was expected to show synergistic antifungal activity with ZnO NPs. In addition, as thiram have adverse effect on human cells[24,25], hepatic system[26], reproductive system[27], and was high toxicity to fish[28] and non-target bacteria[29], we employed *thiram* in our investigation for enhancing its pesticides efficiency and minimizing the negative influence on human health and environment.

Our following experiments firstly established a composite antifungal system that successfully showed the synergistic antifungal activity of ZnO NPs with *thiram*. Furthermore, the photocatalytic degradation of *thiram* under simulated sunlight irradiation ensured eliminating hazardous *thiram* residue. 0.25 g/L ZnO NPs and 0.01 g/L *thiram* were selected as the optimal concentrations for above two components. Infrared spectroscopy, zeta potential analysis and scanning electron microscopy indicated the formation of ZnO-*thiram* antifungal

system, electrostatic adsorption of ZnO NPs to fungi cells and the cellular internalization of ZnO-*thiram* composite played important roles in enhancing antifungal activity. Oxidative stress test showed *thiram* could enhance the ZnO-induced oxidative damage to fungi cells that finally result in synergistic antifungal effect. These achievements offered the opportunity to establish the residue-free green nanotechnology. It is necessary to note that this green nanotechnology has both great economic returns and social benefits by tremendously decreasing the potential adverse influence on environment and public health.

Results

Preparation of composite antifungal system. Characterization of ZnO NPs used in investigation was provided in Supplementary Section 1. The sizes of ZnO NPs were around 20 nm (Supplementary Figure S1b). The surface charge of ZnO NPs was +20.7 mV and + 15.9 mV in antifungal system and deionized water respectively (Supplementary Figure S1c). Pre-treated ZnO NPs with deionized water enabled adsorption of H_2O to particles surface that avoid binding unwanted organic molecule. Due to the stronger binding interaction of sulfur atom than oxygen with zinc atom, *thiram* molecule could replace water molecule and therefore assembled onto ZnO NPs surface to form composite antifungal system after adding *thiram* into ZnO NPs suspensions. Infrared Spectroscopy (IR) analysis was performed to study the interaction between the ZnO NPs and *thiram*. In Figure 1, the absorption located at 428 cm^{-1} is the characteristic ZnO absorption. Peaks of *thiram* at 1374, 1235 cm^{-1} are assigned to stretching vibration and flexural vibrations of C=S. Peak at 1374 cm^{-1} is assigned to the symmetric deforming vibration of $-CH_3$. After mixing with ZnO NPs, IR spectrum of *thiram* samples changed at some peaks. For example, peaks at 1374 cm^{-1} disappeared, peaks at 848, 1374, 1505 and 1578 cm^{-1} were observed blue-shift for 20, 5, 27, 53 cm^{-1} respectively. These changes in IR spectrum indicated the weak interaction between ZnO NPs with *thiram* molecules. IR analysis verified our assumption that the sulfur atoms of C=S in *thiram* molecule may bind with Zn atom on the surface of ZnO NPs. As a result, composite antifungal systems formed, which were made of ZnO core and surrounding *thiram* molecules.

Synergistic antifungal activity of ZnO NPs with pesticide *thiram*. ZnO NPs and *thiram* displayed dose-dependent inhibition on hyphal growth of *Phytophthora capsici* (Figure 2a and Figure 2b). Figure 2c shows the antifungal activity of *thiram* in the presence of 0.25 g/L ZnO NPs. In general, ZnO NPs enhanced the antifungal activities of *thiram* under all tested concentrations. Calculating synergy factor (SF) by Abbortt method is a simple way to assess the interaction between the two components. The SFs for 0.25 g/L ZnO NPs with 0.00125, 0.0025, 0.005, 0.01 g/L *thiram* are 0.73, 1.15, 1.38 and 1.71 respectively. The SF for 0.02 g/L *thiram* with ZnO NPs was not calculated because Abbortt method is not suited for high control level *thiram* concentration[16]. Generally the synergy is identified when SF $\geq$ 1.5[16], so only the 0.25 g/L ZnO with 0.01 g/L *thiram* demonstrated synergistic interaction as its SF= 1.71. Thus, 0.01 g/L *thiram* was used for further investigation to evaluate the influence of ZnO NPs concentration on synergistic effect. As been shown in Figure 2d, ZnO NPs of all the concentrations greatly increased the antifungal activities of 0.01 g/L *thiram*. The inhibition rates were 87%, 95%, 100%, 100%, 100% for 0.05, 0.1, 0.25, 0.5, 1.0 g/L ZnO with 0.01 g/L *thiram* respectively. The SF were 1.95, 1.72, 1.7 and 1.5 for 0.05, 0.1, 0.25, 0.5 g/L ZnO with 0.01 g/L *thiram* respectively, so it can be concluded that ZnO NPs could synergistically enhance the antifungal acitivity of 0.01 g/L *thiram*. The SF of 1.0 g/L ZnO with 0.01 g/L *thiram* was not calculated due to the excessive inhibition rate of single ZnO. FICIs were also determined to verify the results derived from Abbortt method. According to the MICs of ZnO NPs, *thiram* and their combinations, the FICIs of 0.05, 0.1, 0.25, 0.5 g/L ZnO NPs combined with 0.01 g/L *thiram* were 0.275, 0.3, 0.375 and 0.5 respectively, which are lower than or equal to 0.5[15], suggesting synergistic antifungal effect. This result was consistent with conclusion defined by Abbortt method. According to above results, 0.25 g/L ZnO NPs was considered as the optimal dosage for getting a complete control of plant pathogen *Phytophthora capsici* growth with lowest ZnO NPs input. It also can be concluded that *thiram* concentration played a key role in defining the interaction mode of ZnO-*thiram* joint antifungal activity. The comprehensive investigation on antifungal activities of *thiram* in the presence of various ZnO NPs concentrations is demonstrated in Supplementary Section 2.

Photocatalytic degradation of pesticide *thiram* by ZnO NPs. For the purpose of establishing a residue-free green synergistic antifungal nanotechnology we emphasized at the beginning, the photocatalytic degradation of *thiram* in the presence of the ZnO NPs were investigated under simulated sunlight irradiation by a 500 W Xeon lamp. At first, we investigated the effect of catalyst concentration on degradation rates of *thiram*. Because 0.05, 0.1, 0.25, 0.5 g/L ZnO NPs synergistically enhanced the antifungal activity of 0.01 g/L *thiram*, such concentrations were used for degradation study. As been shown in Figure 3a, it is obvious that the efficiency increased with increasing ZnO NPs concentration up to 0.25 g/L. However, the degradation efficiency maintained when the catalyst amount continued increased

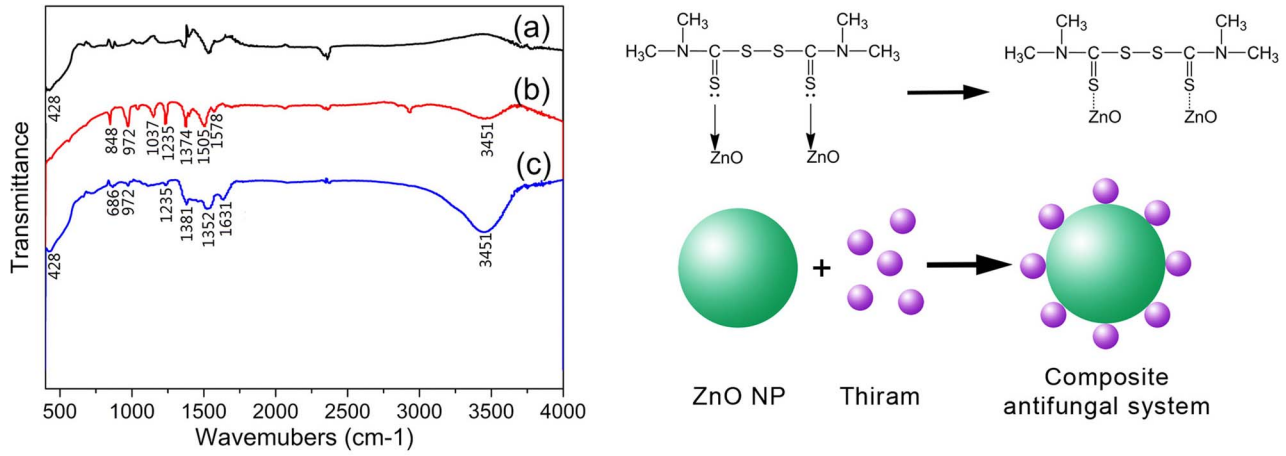

Figure 1 | IR spectra of ZnO (a), *thiram* (b), ZnO-*thiram* (c) and Schematic diagram of ZnO NPs combined *thiram* to form composite antifungal system.

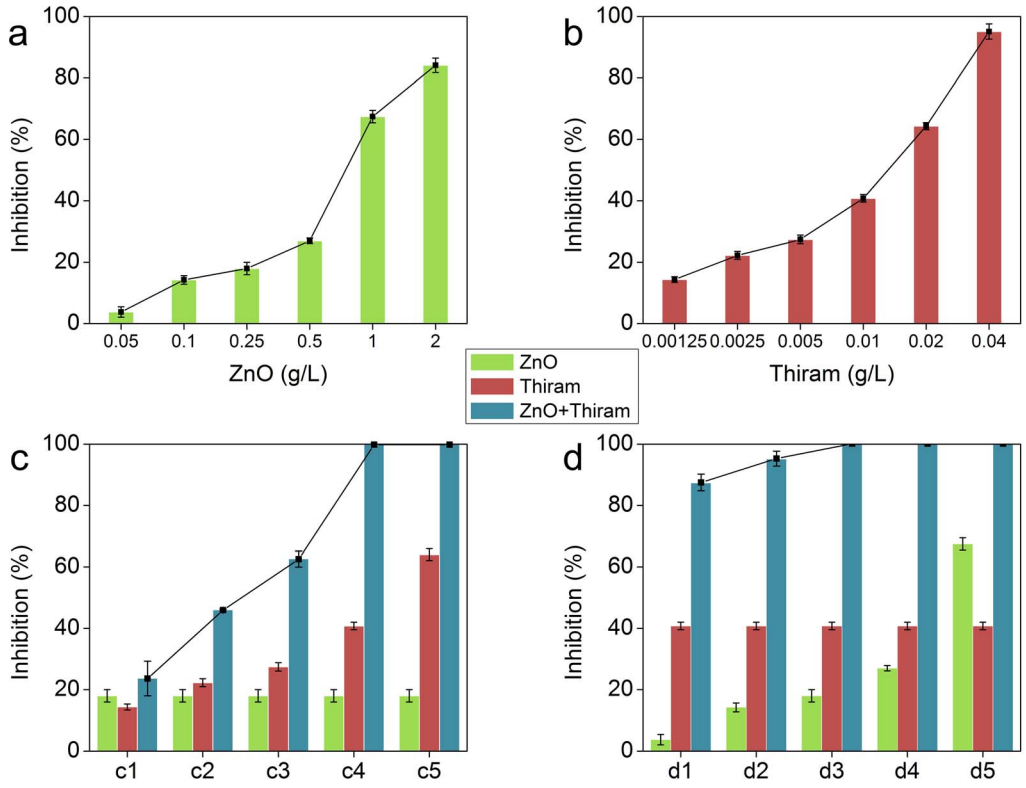

Figure 2 | Antifungal activities of ZnO NPs, *thiram* and ZnO-*thiram*. Part a, Antifungal activity of ZnO NPs alone. Part b, Antifungal activity of *thiram* alone. Part c, Antifungal activity of 0.25 g/L ZnO NPs with increasing *thiram* concentrations. (c1) 0.25 g/L ZnO (green column), 0.00125 g/L *thiram* (red column), 0.25 g/L ZnO with 0.00125 g/L *thiram* (blue column); (c2) 0.25 g/L ZnO (green column), 0.0025 g/L *thiram* (red column), 0.25 g/L ZnO with 0.0025 g/L *thiram* (blue column); (c3) 0.25 g/L ZnO (green column), 0.005 g/L *thiram* (red column), 0.25 g/L ZnO with 0.005 g/L *thiram* (blue column); (c4) 0.25 g/L ZnO (green column), 0.01 g/L *thiram* (red column), 0.25 g/L ZnO with 0.01 g/L *thiram* (blue column); (c5) 0.25 g/L ZnO (green column), 0.02 g/L *thiram* (red column), 0.25 g/L ZnO with 0.02 g/L *thiram* (blue column). Part d, Antifungal activity of 0.01 g/L *thiram* with increasing ZnO concentrations. (d1) 0.05 g/L ZnO (green column), 0.01 g/L *thiram* (red column), 0.05 g/L ZnO with 0.01 g/L *thiram* (blue column); (d2) 0.1 g/L ZnO (green column), 0.01 g/L *thiram* (red column), 0.1 g/L ZnO with 0.01 g/L *thiram* (blue column); (d3) 0.25 g/L ZnO (green column), 0.01 g/L *thiram* (red column), 0.25 g/L ZnO with 0.01 g/L *thiram* (blue column); (d4) 0.5 g/L ZnO (green column), 0.01 g/L *thiram* (red column), 0.5 g/L ZnO with 0.01 g/L *thiram* (blue column); (d5) 1.0 g/L ZnO (green column), 0.01 g/L *thiram* (red column), 1.0 g/L ZnO with 0.01 g/L *thiram* (blue column). Error bars are standard errors with n = 3.

to 0.5 g/L. These results were in accord with previous report that the efficiency became nearly flat even decreased when the catalyst concentration above a certain level[30]. Theoretically, increasing the concentration of the catalyst causes an increase in the degradation rate through providing more active site of the catalyst and accelerates the generation of hydroxyl radical[31], whereas, above certain amount, the excessive ZnO NPs decrease light penetration and increase particles agglomeration[32,33] that finally leading to decreased catalytic efficiency. These finding suggested the optimal usage of ZnO NPs was 0.25 g/L, which synergistically inhibited the fungal growth by over 90% as well as degraded *thiram* residue to safety level efficiently. Figure 3b shows completely photocatalytic degradation of *thiram* by 0.25 g/L ZnO NPs, the absorbance of *thiram* at 278 nm drop below zero (−0.0013) which is lower than the detection limit (0.00122), suggesting the *thiram* was totally degraded. The effect of thiram concentration on degradation rates is shown in Figure 3c, it was observed that the degradation efficiency decreased with increasing *thiram* concentration. This finding suggested a prolonged photocatalytic degradation process required for removing residue at higher *thiram* dosage. This effect of initial substrate concentration on degradation rates may be illustrated by the fact that a larger number of *thiram* molecules competed for the adsorption sites, consequently that production of oxidative radicals were insufficient and the degradation rate was reduced[34].

Morphological analysis of fungal growth. The interaction between ZnO NPs and fungi cells may altered the morphology of fungal samples[18,19]. Thus, Scanning electron microscopy (SEM) analysis was performed to investigate the influence of antifungal agents on fungal structure and provide useful information of mechanism of antifungal activity. No obvious change of fungal hyphae morphology was detected in 0.0025 g/L *thiram* sample (Figure 4b) compared with control (Figure 4a). Diminishing in net framework and reduced density of hyphae were observed after they were treated with 1.0 g/L ZnO NPs (Figure 4c). These result indicates intense inhibition on hyphae growth (Figure 4c). Changes in hyphae structures were found at the backside of the agar plates with some irregular objects presented on hyphae (Figure 4d). Under high magnification observation, it was observed the irregular objects connected with hyphae smoothly (Figure 4e), which inidicated these abnormal enlargements were part of hyphae rather than simply attaching on the hyphae. The same morphological changes with abnormal enlargement of hyphae were also found in ZnO-*thiram* samples (Figure 4f and Figure 4g). Energy-dispersive X-ray (EDX) analysis was performed at the abnormal enlargements of hyphae in pure ZnO treatments. Zincs were found on such enlargements (Figure 4h). This result implied the cellular internalization of ZnO NPs by *Phytophthora capsici*. Because ZnO NPs could not be digested or metabolized by fungi cells, the accumulating of ZnO

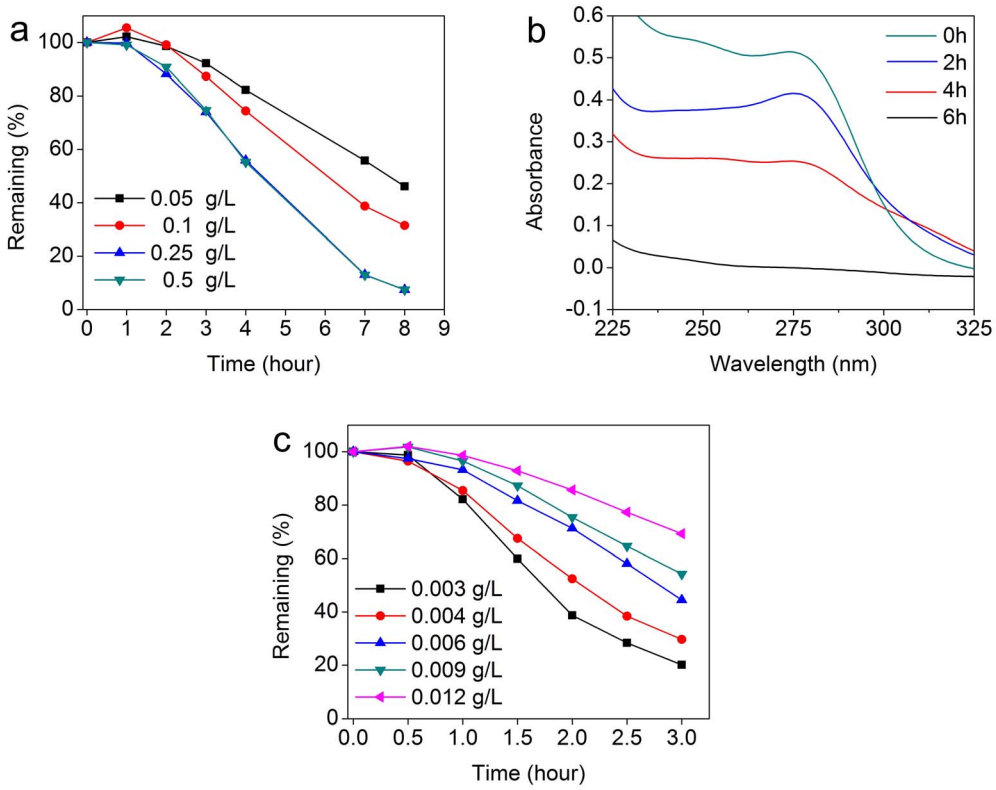

Figure 3 | Photocatalytic degradation of *thiram* under continuous stimulated sunlight irradiation. (a) Effect of ZnO NPs concentration on photocatalytic degradation of *thiram*. (b) Completely photocatalytic degradation of *thiram* in the presence of 0.25 g/L ZnO NPs. The absorption curve of thiram became nearly flat after 6 h irradiation. (c) Effect of initial *thiram* concentration on photocatalytic degradation of *thiram*.

NPs at someplace in hyphae therefore led to the formation of abnormal enlargements. Since the ZnO-*thiram* composite formed, *thiram* may enter fungi hyphae with the cellular internalization of ZnO NPs. In order to investigate whether *thiram* deposited on ZnO surface and enter fungi cells with ZnO NPs together, we also used EDX tool to analysis the abnormal enlargements on hyphae in ZnO-*thiram* treated sample. Demonstrated in Figure 4i, the obvious Zn-peaks were found and suggesting the uptake of ZnO NPs by fungi cells. However, the experimental *thiram* concentration was too low (0.0025 g/L), so that the observation of S-peak was difficult. In addition, when ZnO-*thiram* composites entered fungi cells, parts of *thiram* may consequently disassembled and took part into intracellular life activities, therefore, the signal of sulfur was further reduced. In order to figure out the problem, we tried to increase the *thiram* concentration to enhance the signal of sulfur in the *thiram* after entering the hyphae. However, due to the synergistic antifungal effect, increased *thiram* concentration will lead to totally inhibition on hyphae growth which made incapable to analysis hyphae with EDX tool. For this reason, we performed EDX analysis on ZnO-*thiram* composite directly. Seen from Figure 4j, an obvious sulfur peak appeared at 2.20, which indicated that *thiram* successively deposited on the ZnO surface. This was consistent with the IR analysis (Figure 1) and the both result may be confirmed.

Detection of oxidative stress in synergistic antifungal behavior of ZnO NPs with *thiram*. Some researches indicated the generation of reactive oxygen species (ROS) as the main mechanism responsible for the antimicrobial activity of nano ZnO[13,18,35,36]. The generation of ROS such as hydroxyl radical ($^{\cdot}OH$), superoxide ($O_2^{\cdot-}$) and hydrogen peroxide (H_2O_2)[37,38], induce oxidative stress which can damage cell membranes, nucleic acids and cellular proteins, may lead to cell death[41]. In our experiment, the oxidative stress was detected in carrot broth containing ZnO NPs, results are showed in Supplementary Section 3, and it suggested the level of oxidative stress correlated to the concentration of ZnO NPs.

In order to investigate the oxidative damage toward fungi cells induced by ZnO NPs, histidine was used in our investigation for its antioxidant property. Histidine was reported to protect living cells against oxidative damage through scavenging free radicals[39,40]. Optimal usage of histidine was determined according to condition experiment (Supplementary Section 4). In our investigation (Figure 5a), histidine reduced the inhibition rate of fungal growth of both ZnO and ZnO-*thiram* samples. However, the protective effect of histidine to fungi was more significant in ZnO samples than in ZnO-*thiram* with reductions of antifungal activities by 24% and 13% respectively. These findings confirmed the oxidative damage to fungi hyphae from ZnO NPs in another aspect. It also can be concluded that the combination of ZnO with *thiram* enhanced the oxidative stress and damage to fungi cells.

As living cell possess a cellular defense system including antioxidant enzymes such as SOD to scavenge and prevent damages caused by ROS[18], the SOD activities generally reflected the oxidative stress endured by living cell. Thus, SOD assay was introduced to detect the response of fungi cells exposed to oxidative stress and investigate the mechanism of synergistic antifungal activity of ZnO-*thiram* composite antifungal system. Interestingly, the SOD activities increased in a dose-dependent manner was observed (Supplementary Figure S5), 41.0, 58.5 and 100.7 U/mg protein of SOD activity were detected in 0.5, 1.0 and 2.0 g/L ZnO NPs samples respectively, in contrast, the control set was 28.1 U/mg protein of SOD activity. This finding suggested that ZnO NPs induced the formation of ROS and imposed oxidative stress to fungi cells. Similar results was reported by Patra et al[18] that ZnO NPs induce the increase of SOD activity in two fungi strains. Further experiments were conducted to investigate the influence of *thiram* and ZnO-*thiram* combination. It was found 0.0025 g/L *thiram* did not induce an increasing of SOD activity, instead, it

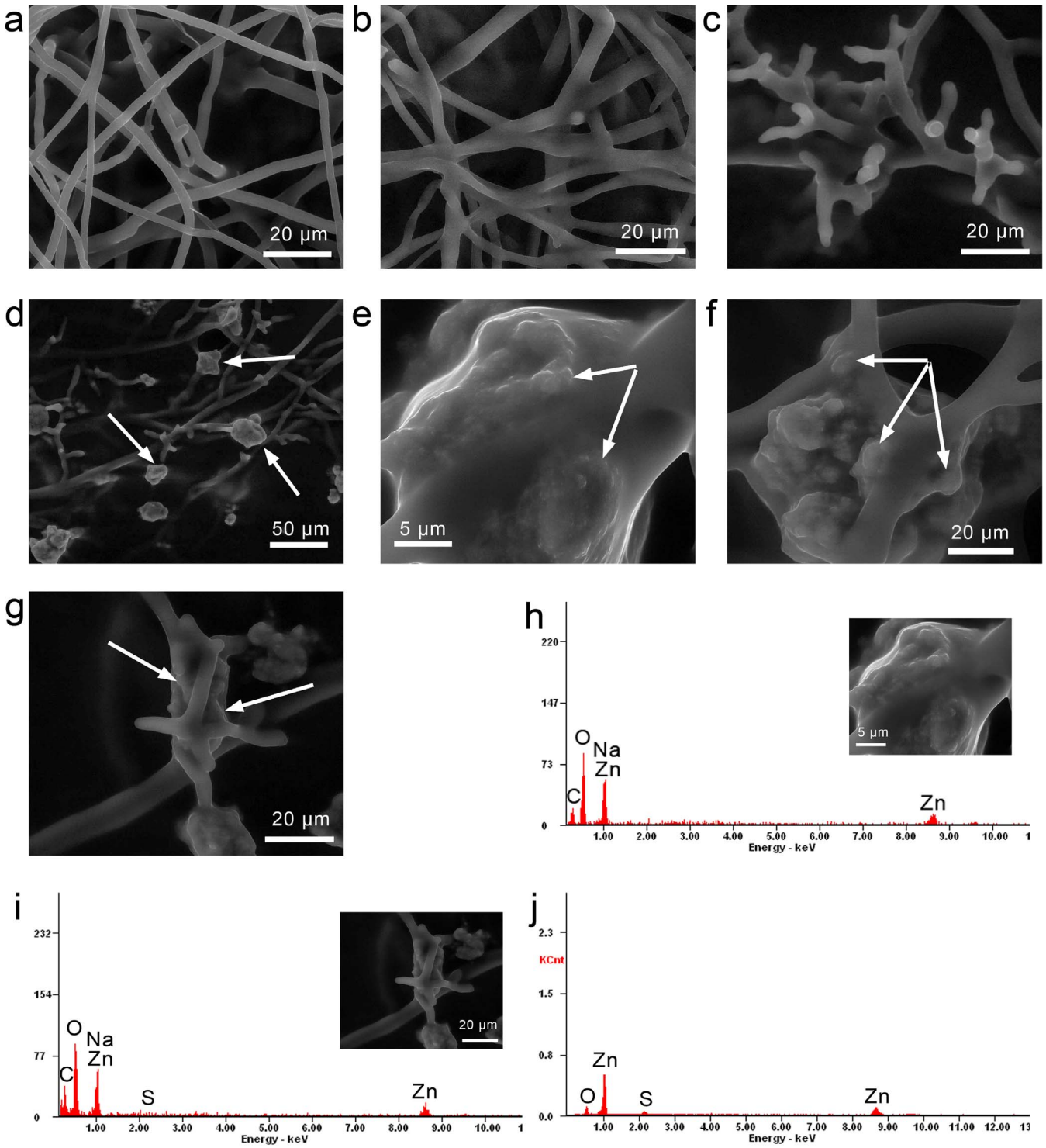

Figure 4 | SEM study and EDX analysis of ZnO NPs and ZnO-*thiram* treated fungi hyphae. SEM showed the inhibition of fungi hypha growth and abnormal enlargements (white arrows) on hypha in the presence of ZnO NPs and ZnO-*thiram* composites: (a) control, (b) 0.0025 g/L *thiram*, (c–e) 1.0 g/L ZnO, (f and g) 1.0 g/L ZnO with 0.0025 g/L *thiram*. EDX analysis performed on abnormal enlargements on hyphae: (h) 1.0 g/L ZnO treatment, (i) 1.0 g/L ZnO with 0.0025 g/L *thiram* treatment, (j) EDX analysis performed on ZnO-*thiram* composite directly.

slightly reduced SOD activity compared to control (Figure 5b). It was speculated that the toxicity of *thiram* to *Phytophthora capsici* was not based on formation of oxidative stress. However, investigation demonstrated that when 0.0025 g/L *thiram* was introduced into 1.0 g/L ZnO NPs, the SOD activity level (91.0 U/mg protein) was higher than 1.0 g/L ZnO NPs treatment alone. This result confirmed antioxidant test that ZnO-*thiram* treatment stimulated an enhanced oxidative stress on fungi cells compared to ZnO NPs alone.

Discussion

To the best of our knowledge, it is the first time to report synergistic antifungal effect of semiconductor NPs with pesticide. Synergy between antibiotics may generate from several pathways[15,23]. According to IR analysis (Figure 1), we demonstrated the formation of composite antifungal system by weak interaction between ZnO NPs and *thiram*. This led to the increasing *thiram* concentration at active sites where antifungal agents contacted with pathogen fungi

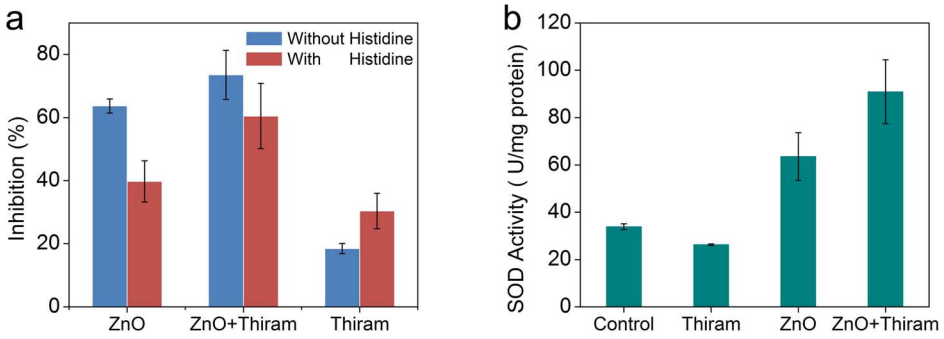

Figure 5 | Oxidative stress study of ZnO and ZnO-*thiram* treated samples. (a): Effect of antioxditant histidine on antifungal activity of 1.0 g/L ZnO, 1.0 g/L ZnO with 0.0025 g/L *thiram*, 0.0025 g/L *thiram*. Reductions of antifungal activities were 24% and 13% respectively for ZnO and ZnO-*thiram* samples. However, no protective effect was observed in *thiram* sample. (b): SOD activities of fungi cells in the presence of 0.0025 g/L *thiram*, 1.0 g/L ZnO and 1.0 g/L ZnO with 0.0025 g/L *thiram*. It shows ZnO-thiram treated sample exhibits a higher SOD activity than ZnO treated alone. The above two test suggest the ZnO-induced oxidative damage were enhanced by *thiram*. Error bars are standard errors with n = 3.

and therefore caused more destruction. Generally, the fungi surface is negative charged at biological pH[41,42] due to the arrangement of the carboxyl and phosphate groups on the cell walls. Thus, positive charged ZnO NPs (Supplementary Figure S1c) were considered to have close physical interaction with fungi cells by direct electrostatic adsorption. As a result, cell membrane damage[43] and cellular internalization were promoted. The cellular internalization of ZnO NPs was confirmed by SEM and EDX analysis (Figure 4). The penetration of ZnO NPs could cause more ZnO-induced oxidative damage intracellular than outside the cells. Meanwhile, as the ZnO-*thiram* composites formed, the uptake of ZnO NPs could help *thiram* entering the fungi cells that promote to exert *thiram* toxicity. When ZnO-*thiram* composite enter fungi cells, it is important to investigate their joint effect on cellular life activities for further understanding the mechanism of synergy. Recent studies have shown ZnO NPs induced the generation of ROS which cause oxidative stress[18,36]. Though excessive ROS-generation imposed unacceptable oxidative stress to cells that result in cell damage, small amount ROS can be tolerated by most cell types[38]. However, when ROS defense system be weakened or inactivated, the same amount ZnO NPs could exhibit higher toxicity to fungi cells. The mode of *thiram* action was thought to be a complex process, one of its fungicide effects was considered as the depletion of glutathione (GSH)[44] and intracellular inactivation of glutathione reductase[45] due to the disulfide bridge in the *thiram* structure. GSH plays an important role in cellular life-activity, it has been reported to protect cells against the destructive effects of oxidative stress caused by ROS[46]. Decrease in levels of GSH resulted in more oxidative damage to the fungi cells by the same amount ZnO NPs. GSH was also claimed to modulate critical cellular processes such as transport of amino acids, stabilization of cell membranes[46], regulation of gene expression and apoptosis[47]. Lack of GSH could lead to disturbance in such cellular processes, and finally fungi cells were more vulnerable when exposed to ZnO NPs. Interestingly, as the synergy could only be identified with 0.01 g/L *thiram* rather than with lower *thiram* concentration (Figure 2c), we suggest it is another proof concerning the role of GSH depletion in synergistic antifungal activity of *thiram* with ZnO NPs. The depletion of GSH may be insufficient to reduce the antioxidant capability of fungi at lower *thiram* concentration samples, whereas higher concentration *thiram* damaged the cellular antioxidant system adequately that provided the opportunity for ZnO NPs to develop more oxidative damage to fungi cells. As a result, ZnO NPs exhibited synergistic antifungal activity with *thiram* (Figure 2c and Figure 2d), correspondingly, the protection effect of histidine decreased (Figure 5a), and the SOD activity of fungi cells increased in ZnO-*thiram* samples (Figure 5b).

In conclusion, as been shown in Figure 6, we speculated that the formation of ZnO-*thiram* composite antifungal system, electrostatic adsorption of ZnO-*thiram* groups to fungi cells and the cellular internalization ZnO NPs played important roles in synergistic antifungal activities which facilitate ZnO NPs, *thiram* and their combination interacted with fungi hyphae. As a result, antioxidant capability of fungi cells was weakened, and led to more damage under ZnO-induced oxidative stress, finally the synergistic antifungal activity was obtained against pathogen fungi *Phytophthora capsici*.

Using the synergistic antifungal ZnO-*thiram* concentration ratio, we successfully demonstrated a completely degradation of pesticide *thiram* by ZnO NPs in an aqueous solution system. This entirely removal of organic pollutants by semiconductor NPs was consistent with previous studies of photocatalytic degradation of organic pollutant[48,49]. Generally, photocatalytic experiments were conducted in an aqueous solution system. According to the photocatalytic degradation theory, the deposited *thiram* could be degraded after attacking by photo-generated electron−hole pairs, then released active sites on ZnO were available for free *thiram* molecules. Therefore, the free *thiram* continued depositing/absorbing on ZnO NPs surface and consequently being degraded. Moreover, the photo-generated holes can react with OH^- or H_2O and oxidize them into $^{\cdot}OH$ radicals; meanwhile the photo-generated electrons could react with O_2 adsorbed on the catalyst surface or dissolved in water, and reduce it to superoxide radical anion $O_2^{\cdot -}$. These highly oxidative radicals could oxidize free *thiram* existed in the system. As a result, all *thiram* molecules, whether deposited or free, were degraded completely. It is also worthy to mention that even in practical pesticides application, due to the moisture in the air and the transpiration effect of plant, the micro aqueous solution system could formed on leafs and provide photocatalytic reaction system for *thiram* degradation. So *thiram* could also be totally degraded in practical systems.

Combining the synergistic antifungal activity and successive photocatalytic degradation of *thiram*, we established a residue-free green synergistic antifungal nanotechnology for pesticide *thiram* by ZnO NPs. The schematic diagram of the nanotechnology is depicted in Figure 6. Owing to the synergistic antifungal activity, this nanotechnology firstly offers the opportunity to reduce *thiram* usage from 0.04 g/L to 0.01 g/L in the presence of ZnO NPs without compromise in pathogen control. Furthermore, the complete photocatalytic degradation enables the ZnO NPs to remove the excess *thiram* after antifungal process and consequently restrict the *thiram* residue under maximum residue limits set up by government administrations. Such significant decline in *thiram* usage and successive degradation of *thiram* to safety level benefit the human social greatly by providing economic advantage as well as avoiding the negative

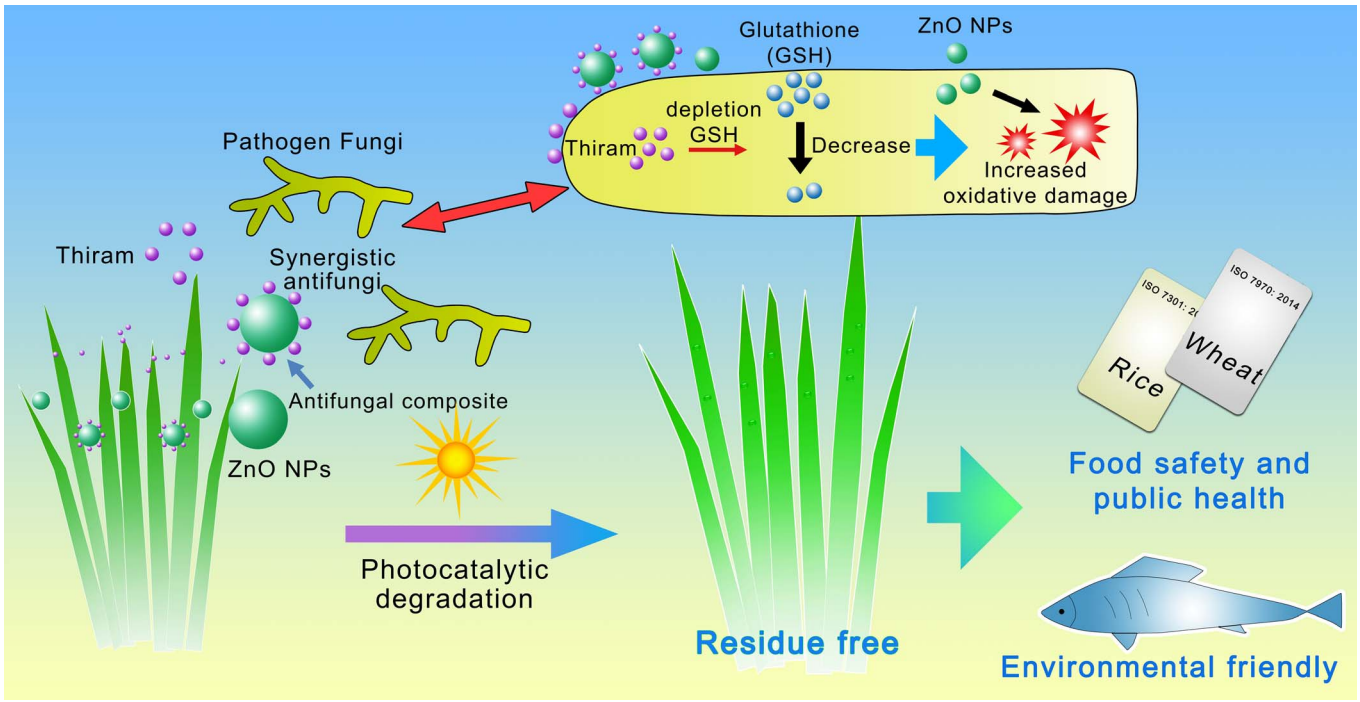

Figure 6 | Schematic diagram of residue-free green nanotechnology enhanced the pesticide efficiency and ensured food safety and public health. Figure 6 and drawings within it were created by author J.Z.X.

impacts on public health and environment. This paper displayed notable effects of our residue-free green nanotechnology, however, more work still need to be done for further deeper understanding the synergistic mechanism and broadening the application range with other pesticides.

Methods

Materials and Characterization. ZnO NPs purchased from Tianxin Zinc Industry Co., Ltd. (Baoji, Shanxi, China) were characterized by X-ray diffraction (XRD) and transmission electron microscopy (TEM). Before antifungal test, ZnO NPs were pre-treated with deionized water. Zeta potential of ZnO NPs was examined by Zetasizer Nano (Malvern, UK). *Thiram* used in this study was purchased from Sinopharm Chemical Reagent Co, Ltd. Shanghai China (analytical grade). *Thiram* was added to ZnO NPs water suspension with vigorous shaking to form the composite antifungal system. The assembling of *thiram* on the surface of ZnO NPs by weak binding was characterized by infrared spectroscopy (Nicolet 6700, Thermo, USA). Carrot agar (CA) medium (juice of 200 g fresh carrot and 13 g agar in 1000 mL distill water) were prepared for fungal cultivation and antifungal test.

Antifungal test. Pathogenic fungi *Phytophthora capsici* used in this study was obtained from China Agricultural University. Antifungal tests were performed by the mycelial growth rate method in presence of various concentrations of inhibitor. ZnO NPs, thiram and ZnO-thiram combinations were added to melted CA medium at about 45 ± 5°C for evaluating antifungal activities. The mediums were shaken vigorously and then poured into the Petri dishes (9 cm diameter). The fungi were inoculated after the CA medium solidified. Agar plugs (5 mm) obtained from the edge of 7-day-old fungal cultures were placed in the center of each Petri dish. All samples were then incubated at 25°C in the dark. The diameters of fungal colonies were measured after 4 day incubation. All of the samples were prepared in triplicate, and all experiments were repeated twice or more. Antifungal efficacy were calculated as followed method:

Antifungal efficacy = $(Dc - Dt) \times 100\%/Dc$

where Dt = diameter of colonies in test plate; Dc = diameter of colonies in control plate.

The combined antimicrobial effects of pesticides with ZnO NPs could be evaluated by two methods. One is to calculate the expected efficacy of ZnO NPs and *thiram* mixtures by Abbortt formula first:

$\%C_{exp} = A+B-(A \times B/100)$

in which A and B are the control efficacy given by the single pesticide[50]. Then, increased control efficacy of pesticides mixtures (synergy factor, SF) was calculated using formula below[16]:

$SF = \%C_{obs}/\%C_{exp}$

Where $\%C_{obs}$ = observed efficacy. SF ≥ 1.5 showed synergistic effect, SF ≤ 0.5 demonstrated antagonism. Others were addictive effect. Another is the fractional inhibitory concentration index (FICI). The FICIs were calculated by the following equation according to minimum inhibitory concentration (MIC). $FICI = FIC_A + FIC_B = MIC_{comb\cdot A}/MIC_{alone\cdot A} + MIC_{comb\cdot B}/MIC_{alone\cdot B}$, where $MIC_{alone\cdot A}$ and $MIC_{alone\cdot B}$ are the MIC values of drugs *A* and *B* when acting alone, and $MIC_{comb\cdot A}$ and $MIC_{comb\cdot B}$ are the concentrations of drugs *A* and *B* at combinations. The interpretation of the FICI was as follows: a FICI ≤ 0.5 demonstrated synergy; a FICI between 0.5 and 4 indicated no interaction; and a FICI ≥ 4 showed antagonism[15].

Photocatalytic degradation procedure. All photocatalytic experiments were conducted using an SGY-II photochemical reactor purchased from Nanjing Stonetech. EEC Ltd., Nanjing, China. Series of 40 mL *thiram* aqueous solutions of desired concentration were filled in each quartz tubes (50 mL) and required amount ZnO NPs were added. Before irradiation, quartz tubes with sample solutions were subjected to sonication for 20 min to disaggregate ZnO NPs and then placed inside the reactor for 30 min standing to achieve adsorption equilibrium. Magnetic stirrers were located at the base of reactor that a homogenous ZnO NPs suspension could be maintained throughout the reaction. *Thiram* solutions were illuminated with a 500 W Xeon lamp without filters. Samples were collected before and at regular intervals during the irradiation. Analysis were performed, after separation of the photocatalyst particles by centrifugation (3000 rpm, twice), with a UV-Vis spectrophotometer (UV-Vis 8453, Agilent, USA), measuring the absorbance at maximum wavelength 278 nm. The detection limit of the UV-Vis spectrophotometer for our experiment was also determined.

Morphological test of fungal hyphae. Scanning electron microscopy (SEM) was used to examine morphological changes of *Phytophthora capsici* hyphae with or without ZnO NPs treatment. Pieces of fungi hyphae material cut from 7-day-old cultures were inoculated onto the CA medium containing 1.0 g/L ZnO NPs, 0.0025 g/L *thiram*, 1.0 g/L ZnO NPs + 0.0025 g/L *thiram* and control treatment (ZnO-free and *thiram*-free) followed by incubation for 4 days. Then, agar plugs contained fungi hyphae were cut from the edge of the fungal cultures and directly subjected to SEM analysis under the environmental mode. SEM images were taken by FEI Quanta 200F Environmental SEM at a voltage of 20 kV and a pressure 350 Pa.

Inhibitory effect of antioxidant on ZnO NPs antifungal activity. Histidine was reported as a well-known antioxidant which could scavenge hydroxyl radicals and singlet oxygen. In order to determine the Oxidative stress caused by ZnO NPs, histidine were add to CA media which contain 1.0 g/L ZnO, 0.0025 g/L *thiram* and 1.0 g/L ZnO + 0.0025 g/L *thiram* respectively. The fungi were inoculated after the CA media solidified. Inhibition effect of histidine on ZnO antifungal activities were measured after 4-day cultivation.

Superoxide Dismutase (SOD) Catalase activity assay. For SOD assay, fungi mycellial balls were isolated and washed with 0.85% saline solution after 48 h inoculation. The samples were subjected to sonication for 5 min to rupture the fungal cell wall. Homogenate were taken to determine the activities of SOD using assay kits

(Nanjing Jiancheng Bioengineering). Assay was based on determining the inhibition of nitroblue tetrazolium (NBT) reduction due to superoxide anion produced by a xanthine/xanthine oxidase system. One enzyme unit of SOD was defined as that amount of protein (in mg) causing a 50% inhibition of the formation of formazan dye.

1. Verger, Philippe, J. P. & Boobis, A. R. Reevaluate Pesticides for Food Security and Safety. *Science* **341**, 717–718 (2013).
2. Sande, D., Mullen, J., Wetzstein, M. & Houston, J. Environmental Impacts from Pesticide Use: A Case Study of Soil Fumigation in Florida Tomato Production. *Int. J. Env. Res. Pub. He.* **8**, 4649–4661 (2011).
3. Verdisson, S., Couderchet, M. & Vernet, G. Effects of procymidone, fludioxonil and pyrimethanil on two non-target aquatic plants. *Chemosphere* **44**, 467–474 (2001).
4. Alavanja, M. C. R., Hoppin, J. A. & Kamel, F. Health effects of chronic pesticide exposure: Cancer and neurotoxicity. *Annu. Rev. Publ. Health* **25**, 155–197 (2004).
5. Juraske, R., Mutel, C. L., Stoessel, F. & Hellweg, S. Life cycle human toxicity assessment of pesticides: Comparing fruit and vegetable diets in Switzerland and the United States. *Chemosphere* **77**, 939–945 (2009).
6. Eddleston, M. *et al*. Pesticide poisoning in the developing world—a minimum pesticides list. *The Lancet* **360**, 1163–1167 (2002).
7. Tilman, D., Cassman, K. G., Matson, P. A., Naylor, R. & Polasky, S. Agricultural sustainability and intensive production practices. *Nature* **418** (6898), 671–677 (2002).
8. Panacek, A. *et al*. Antifungal activity of silver nanoparticles against Candida spp. *Biomaterials* **30**, 6333–6340 (2009).
9. Applerot, G. *et al*. Understanding the Antibacterial Mechanism of CuO Nanoparticles: Revealing the Route of Induced Oxidative Stress. *Small* **8**, 3326–3337 (2012).
10. Makhluf, S. *et al*. Microwave-assisted synthesis of nanocrystalline MgO and its use as a bacteriocide. *Adv. Funct. Mater.* **15**, 1708–1715(2005).
11. Brayner, R. *et al*. Toxicological impact studies based on Escherichia coli bacteria in ultrafine ZnO nanoparticles colloidal medium. *Nano Lett.* **6**, 866–870 (2006).
12. Li, Y., Zhang, W., Niu, J. F. & Chen, Y. S. Mechanism of Photogenerated Reactive Oxygen Species and Correlation with the Antibacterial Properties of Engineered Metal-Oxide Nanoparticles. *ACS Nano* **6**, 5164–5173 (2012).
13. Applerot, G. *et al*. Enhanced Antibacterial Activity of Nanocrystalline ZnO Due to Increased ROS-Mediated Cell Injury. *Adv. Funct. Mater.* **19**, 842–852 (2009).
14. Li, P., Li, J., Wu, C. Z., Wu, Q. S. & Li, J. Synergistic antibacterial effects of beta-lactam antibiotic combined with silver nanoparticles. *Nanotechnology* **16**, 1912–1917 (2005).
15. Luo, Z. H., Wu, Q. S., Xue, J. Z. & Ding, Y. P. Selectively Enhanced Antibacterial Effects and Ultraviolet Activation of Antibiotics with ZnO Nanorods Against Escherichia Coli. *J. Biomed. Nanotechnol.* **9**, 69–76 (2013).
16. Gisi, U. Synergistic interaction of fungicides in mixtures. *Phytopathology* **86**, 1273–1279 (1996).
17. Zhang, L. L., Jiang, Y. H., Ding, Y. L., Povey, M. & York, D. Investigation into the antibacterial behaviour of suspensions of ZnO nanoparticles (ZnO nanofluids). *J. Nanopart. Res.* **9**, 479–489 (2007).
18. Patra, P., Mitra, S., Debnath, N. & Goswami, A. Biochemical-, Biophysical-, and Microarray-Based Antifungal Evaluation of the Buffer-Mediated Synthesized Nano Zinc Oxide: An in Vivo and in Vitro Toxicity Study. *Langmuir* **28**, 16966–16978(2012).
19. He, L. L., Liu, Y., Mustapha, A. & Lin, M. S. Antifungal activity of zinc oxide nanoparticles against Botrytis cinerea and Penicillium expansum. *Microbiol. Res.* **166**, 207–215 (2011).
20. Mitra, S. *et al*. Porous ZnO nanorod for targeted delivery of doxorubicin: in vitro and in vivo response for therapeutic applications. *J. Mater. Chem.* **22**, 24145–24154 (2012).
21. Fakhar-e-Alam, M. *et al*. The potential applications of ZnO nanoparticles conjugated with ALA and photofrin as a biomarker in HepG2 cells. *Laser Phys.* **21**, 2156–2164 (2011).
22. Lu, F., Cai, W. P. & Zhang, Y. G. ZnO hierarchical micro/nanoarchitectures: solvothermal synthesis and structurally enhanced photocatalytic performance. *Adv. Funct. Mater.* **18**, 1047–1056 (2008).
23. Fayaz, A. M. *et al*. Biogenic synthesis of silver nanoparticles and their synergistic effect with antibiotics: a study against gram-positive and gram-negative bacteria. *Nanomed. Nanotechnol. Biol. Med.* **6**, 103–109 (2010).
24. Cereser, C., Boget, S., Parvaz, P. & Revol, A. An evaluation of thiram toxicity on cultured human skin fibroblasts. *Toxicology* **162**, 89–101 (2001).
25. Santovito, A., Cervella, P. & Delpero, M. Chromosomal aberrations in cultured human lymphocytes treated with the fungicide, Thiram. *Drug Chem. Toxicol.* **35**, 347–351 (2012).
26. Dalvi, R. R. *et al*. Thiram-induced toxic liver-injury in male sprague-dawley rats. *J. Environ. Sci. Heal. B.* **19**, 703–712 (1984).
27. Bretveld, R. W., Thomas, C. M. G., Scheepers, P. T. J., Zielhuis, G. A. & Roeleveld, N. Pesticide exposure: the hormonal function of the female reproductive system disrupted? *Reprod. Biol. Endocrin.* **4**, 30 (2006).
28. Sharma, V. K., Aulakh, J. S. & Malik, A. K. Thiram: degradation, applications and analytical methods. *J. Environ. Monitor.* **5**, 717–723 (2003).
29. Milenkovski, S., Baath, E., Lindgren, P. E. & Berglund, O. Toxicity of fungicides to natural bacterial communities in wetland water and sediment measured using leucine incorporation and potential denitrification. *Ecotoxicology* **19**, 285–294 (2010).
30. Cao, Y. S. *et al*. Photocatalytic degradation of chlorfenapyr in aqueous suspension of TiO_2. *J. Mol. Catal. A-Chem.* **233**, 61–66 (2005).
31. Saien, J. & Khezrianjoo, S. Degradation of the fungicide carbendazim in aqueous solutions with UV/TiO_2 process: Optimization, kinetics and toxicity studies. *J. Hazard Mater.* **157**, 269–276 (2008).
32. Daneshvar, N., Aber, S., Dorraji, M. S. S., Khataee, A. R. & Rasoulifard, M. H. Photocatalytic degradation of the insecticide diazinon in the presence of prepared nanocrystalline ZnO powders under irradiation of UV-C light. *Sep. Purif. Technol.* **58**, 91–98 (2007).
33. Nagaveni, K., Sivalingam, G., Hedge, M. S. & Madras, G. Solar photocatalytic degradation of dyes: high activity of combustion synthesized nano TiO_2. *Appl. Catal. B-Environ.* **48**, 83–93 (2004).
34. Daneshvar, N., Salari, D. & Khataee, A. R. Photocatalytic degradation of azo dye acid red 14 in water: investigation of the effect of operational parameters. *J. Photoch. Photobio. A.* **157**, 111–116 (2003).
35. Xia, T. *et al*. Comparison of the Mechanism of Toxicity of Zinc Oxide and Cerium Oxide Nanoparticles Based on Dissolution and Oxidative Stress Properties. *ACS Nano* **2**, 2121–2134 (2008).
36. Lipovsky, A., Nitzan, Y., Gedanken, A. & Lubart, R. Antifungal activity of ZnO nanoparticles-the role of ROS mediated cell injury. *Nanotechnology* **22**, 105101 (2011).
37. Yan, L., Gu, Z. J. & Zhao, Y. L. Chemical Mechanisms of the Toxicological Properties of Nanomaterials: Generation of Intracellular Reactive Oxygen Species. *Chem-Asian J.* **8**, 2342–2353 (2013).
38. Soenen, S. J. *et al*. Cellular toxicity of inorganic nanoparticles: Common aspects and guidelines for improved nanotoxicity evaluation. *Nano Today* **6**, 446–465 (2011).
39. Lee, John, W. *et al*. Improved functional recovery of ischemic rat hearts due to singlet oxygen scavengers histidine and carnosine. *J. Mol. Cell. Cardiol.* **31**, 113–121 (1999).
40. Bersuder, P., Hole, M. & Smith, G. Antioxidants from a heated histidine-glucose model system. I: Investigation of the antioxidant role of histidine and isolation of antioxidants by high-performance liquid chromatography. *J. Am. Oil. Chem. Soc.* **75**, 181–187 (1998)
41. Dunlap, C. A., Biresaw, G. & Jackson, M. A. Hydrophobic and electrostatic cell surface properties of blastospores of the entomopathogenic fungus. *Paecilomyces fumosoroseus. Colloid. Surface B.* **46**, 261–266 (2005).
42. Lee, S. A. *et al*. Assessment of electrical charge on airborne microorganisms by a new bioaerosol sampling method. *J. Occup. Environ. Hyg.* **1**, 127–138 (2004).
43. Espitia, P. J. P. *et al*. Zinc Oxide Nanoparticles: Synthesis, Antimicrobial Activity and Food Packaging Applications. *Food Bioprecess. Tech.* **5**, 1447–1464 (2012).
44. Kim, J. H. *et al*. Chemosensitization of fungal pathogens to antimicrobial agents using benzo analogs. *Fems. Microbiol. Lett.* **281**, 64–72 (2008).
45. Elskens, M. T. & Penninckx, M. J. Thiram and dimethyldithiocarbamic acid interconversion in Saccharomyces cerevisiae: a possible metabolic pathway under the control of the glutathione redox cycle. *Appl. Environ. Microb.* **63**, 2857–2862 (1997).
46. Meister, A. Selective modification of glutathione metabolism. *Science* **220**, 472–477 (1983).
47. Grosicka, E. *et al*. Effect of glutathione depletion on apoptosis induced by thiram in Chinese hamster fibroblasts. *Int. Immunopharmacol.* **5**, 1945–1956 (2005).
48. Zhang, D., Li, J., Wang, Q. G. & Wu, Q. S. High {001} facets dominated BiOBr lamellas: facile hydrolysis preparation and selective visible-light photocatalytic activity. *J. Mater. Chem. A.* **1**, 8622–8629 (2013).
49. Bai, H. *et al*. Large-Scale, Three-Dimensional, Free-Standing, and Mesoporous Metal Oxide Networks for High-Performance Photocatalysis. *Sci. Rep.* **3**, 2204 (2013).
50. Evenhuis, A., Schepers, Htam, Bus, C. B. & Stegeman, W. Synergy of cymoxanil and mancozeb when used to control potato late blight. *Potato Res.* **39**, 551–559 (1996).

Acknowledgments

The authors are grateful to the financial support of the National Natural Science Foundation of China (Nos. 91122025, 21103127, 21101118), the Nano-Foundation of Shanghai in China (No. 11nm0501300), the State Key Laboratory of Fine Chemicals (No. KF1103), the State Major Research Plan (973) of China (No. 2011CB932404), and the Shanghai Key Laboratory of Molecular Catalysis and Innovative Materials (No. 2012MCIMKF03).

Author contributions

J.Z.X., Y.P.D. and Q.S.W. conceived and designed the experiments. J.Z.X., Z.H.L., P.L. and Y.P.D. performed the experiments. J.Z.X., Y.P.D. and Q.S.W. analyzed the data. J.Z.X., Y.C. and Q.S.W. prepared the manuscript.

Additional information

Supplementary information accompanies this paper at http://www.nature.com/scientificreports

Competing financial interests: The authors declare no competing financial interests.

How to cite this article: Xue, J.Z. *et al.* A residue-free green synergistic antifungal nanotechnology for pesticide *thiram* by ZnO nanoparticles. *Sci. Rep.* **4**, 5408; DOI:10.1038/srep05408 (2014).